Dalton Transactions

PAPER

Quantification of Energy Transfer in Bimetallic Pt(II)–Ln(III) Complexes Featuring an N^C^N-Cyclometallating Ligand

Isaac M. Etchells,[a] Michael C. Pfrunder, [a] J. A. Gareth Williams,[b] and Evan G. Moore[a]*

Received 00th January 20xx,
Accepted 00th January 20xx

DOI: 10.1039/x0xx00000x

www.rsc.org/

Cyclometallated Pt(II) complexes with arylpolypyridyl ligands have impressive photophysical properties (high quantum yields, long lifetimes and tuneable emission) which can be readily tuned by modification of the organic ligand. Despite this, few examples of cyclometallated Pt(II) complexes as sensitisers for Ln(III) emission have been reported. Herein, we report the photophysical properties of a series of bimetallic complexes incorporating an N^C^N-coordinated Pt(II) bearing an alkynyl terpyridine as a metalloligand for a Ln(III) ion (where Ln = Nd, Gd, Er, Yb and Lu). Using a combination of steady state, time-resolved, and transient absorption experiments, the influence on the photophysical properties of the metalloligand exerted by the different Ln(III) cations has been investigated, together with the energy transfer efficiency from the metalloligand to the Ln(III) 4*f** excited state.

Introduction

Since the appearance of early reports[1] describjing multimetallic *d-f* complexes with interesting photoluminescence properties, the available catalogue of transition metal complexes which have been used as sensitisers for Ln(III) emission has expanded immensely. Due to their long-lived excited states, there has been a particular focus on photoactive Ru(II), Os(II), and Ir(III) polypyridyl complexes,[2] which can facilitate highly efficient Electronic Energy Transfer (EET) to the excited states of chelated 4*f** cations, resulting in their characteristic luminescence. Moreover, due to the typically lower energy singlet excited states compared to organic sensitisers, longer wavelength excitation in the visible region becomes possible. The relatively low energy of their triplet excited states compared to organic systems has also led to a focus on the use of metal complexes as antennae for the sensitisation of Near Infra-Red (NIR) emitting cations such as Nd(III), Er(III) and Yb(III).

In the majority of cases, the observed NIR emission in these *d-f* complexes relies on Metal to Ligand Charge Transfer (^{3}MLCT) excited states, which are generated by efficient intersystem crossing (ISC). By contrast, for corresponding Pt(II) polypyridyl complexes, the excited states are generally characterised as being 'metal-perturbed' ligand centered states.[3-5] Nonetheless, a variety of Pt(II) polypyridyl luminophores have been used successfully in a range of *d-f* systems, including heterometallic complexes,[6-8] coordination polymers,[9] and supramolecular systems.[10-12] Interestingly then, despite the myriad of Pt(II) polypyridyl-based antennae which have been reported, to the best of our knowledge only two examples of cyclometalated arylpolypyridyl Pt(II) *d-f* complexes[13, 14] have been demonstrated to show sensitised Ln(III) emission. This is surprising, given that the ongoing development of these types of compounds has produced several families of Pt(II) complexes[15-18] which display exceptional photophysical properties. In particular, destabilisation of the Pt(II) centered ligand field (LF) states using cyclometalated complexes such as [Pt(N^C^N)Cl] (N^C^N = 1,3-di(pyridin-2-yl)benzene) can prevent quenching of low-lying ligand-centred triplet excited states due to the presence of the strongly σ-donating ligand, allowing long-lived phosphorescence with high photoluminescence quantum yields (PLQY's) to be obtained[19] when compared to isostructural $[Pt(tpy)Cl]^+$ (tpy = 2,2':6',2''-terpyridine) complexes.[4] In addition, the lifetime and localisation of metal-perturbed π-π* excited states in Pt(II) N^C^N complexes can be influenced by synthetic modification of the parent ligand, or by coordination of additional conjugated ligands at the Pt(II) metal centre. In this way, an increase in conjugation of the ligand system can introduce additional intraligand and/or interligand charge transfer excited states (ILCT), which can also have a significant influence on the resulting photophysical properties.

Given the relatively unexplored potential for these complexes to act as antennae for sensitised lanthanide luminescence, herein we report the steady state and time-resolved luminescence properties of a Pt(II) complex with an N^C^N ligand connected to a Ln(III)-coordinating terpyridine ligand through an ethynyl linker (Scheme 1). Moreover, the excited state dynamics have been investigated using picosecond and nanosecond transient absorption (TA) spectroscopy, in order to elucidate the antenna pathway as well as determine the rate and efficiency of EET for several different Ln(III) cations. This approach can offer numerous advantages compared to techniques based on monitoring photoluminescence, since the residual emission from the donor can often be undetectably weak when the efficiency of EET is very high, or alternately can be convolved with metal based 4*f** emission, which is particularly problematic for visible emitting lanthanides such as Eu(III). Our analysis of the resulting TA data yields EET rate constants on the order of $k_{EET} \approx 10^8$ - 10^9 s^{-1}, and corresponding EET efficiencies from 80 - 98 % for three different NIR-emitting Ln(III) cations.

[a] *School of Chemistry and Molecular Biosciences, University of Queensland, St Lucia, QLD 4072, Australia. E-mail: egmoore@uq.edu.au*
[b] *Department of Chemistry, Durham University, Durham, UK DH1 3LE.*
† Footnotes relating to the title and/or authors should appear here.
Electronic Supplementary Information (ESI) available: [details of any supplementary information available should be included here]. See

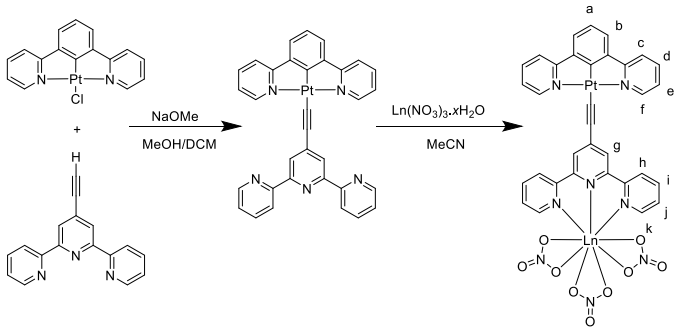

Scheme 1 Synthesis of [Pt(N^C^N)(a-tpy)] metalloligand, and preparation of [Pt(N^C^N)(a-tpy)Ln$(NO_3)_3$] complexes with Ln = Nd, Gd, Er, Yb, and Lu.

Results and Discussion

Synthesis and crystallography

The desired Pt(II) metalloligand was synthesised using a stepwise approach outlined in Scheme 1, from individual components prepared using reported literature methods.[19, 20] Monodentate ligand metathesis between the [Pt(N^C^N)Cl] complex and 4'-ethynyl-2,2':6',2''-terpyridine (a-tpy) was adapted from procedures used to prepare similarly functionalised [Pt(N^C^N)X] complexes where X is a coordinated organic alkyne.[21] The product was obtained in high yield, and was fully characterised by ^{1}H NMR, ESI-MS, CHN and X-ray crystallography. In particular, the crystal structure obtained (Fig. 1) confirms successful preparation of the charge neutral [Pt(N^C^N)(a-tpy)] complex, and reveals that the N^C^N and a-tpy ligands adopt a conformation close to planarity, with only an angle of only 2.2° between the planes of the two organic ligands, which allows for significant π-π packing interactions in the crystal lattice.

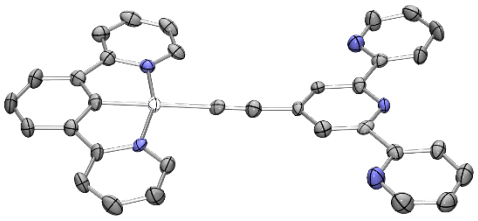

Figure 1: X-ray crystal structure of isolated [(N^C^N)Pt(a-tpy)] complex ($P2_1/c$ R_1 = 3.15 %). H atoms omitted for clarity.

The Pt-N bond lengths of the N^C^N ligand are typical of Pt–pyridine bonds, at *ca*. 2.03 Å, and are longer than the Pt-C bond for this organometallic ligand, at 1.94 Å. Due to the strong *trans* influence of the Pt–C^{NCN} σ bond, the Pt–$C^{acetylide}$ bond linking the metal to the coordinated a-tpy moiety is slightly longer, at 2.04 Å, than the corresponding bond in Pt(II) terpyridyl acetylides, which is usually around 1.97Å. Notably, the free tpy chelate group has adopted a *trans-trans* configuration of N donor atoms to reduce repulsive interactions between their lone pairs.

Formation and characterisation of *d-f* complexes

Coordination of several different Ln(III) cations to the terpyridyl unit of [Pt(N^C^N)(a-tpy)] in a mixture of CH_3CN:CH_2Cl_2 (3:2 v/v), upon addition of a slight excess of Ln(III) nitrate salts, was confirmed using MS and NMR spectroscopy. As shown in Fig. 2, the ^{1}H NMR spectrum of the free [Pt(N^C^N)(a-tpy)] metalloligand reveals several characteristic resonances in the aromatic region, which were fully assigned using 2D COSY and 1D NOESY techniques (see Fig. S1, ESI). In particular, a 2H signal from the a-tpy 3'/5' protons appears as a sharp singlet at *ca*. 8.53 ppm, while the 6 and 6'' protons adjacent to the terpyridyl N donor atoms appear as doublets at *ca*. 8.72 ppm. Upon titration with diamagnetic $Lu(NO_3)_3.6H_2O$, these peaks clearly shift downfield, appearing at *ca*. 8.88 ppm (see also Fig. S2, ESI). Notably, during the ^{1}H NMR titration, no evidence for formation of an intermediate LnL_2 complex was observed, which is slightly different behaviour compared to a recently reported Ru(II)-Nd(III) complex featuring a terpyridine ligand, but may likely be due to the smaller ionic radius of the Lu(III) cation and the differing solvents utilised.[22] Nonetheless, upon addition of more than 1 molar equivalent of the 4*f* cation, clean formation of the 1:1 complex is clearly demonstrated in the present case. Also shown as an inset of Fig. 2 is the HRMS (ESI+) spectrum of the major peak observed for the Lu(III) complex at *ca.* 980 m/z, together with the calculated isotopic distribution pattern for a $[Pt(N^C^N)(a\text{-}tpy)Lu(NO_3)_2]^+$ fragment, which shows excellent agreement with the experimental spectrum. The remaining paramagnetic complexes with Ln = Nd, Gd, Er, and Yb were also characterised using HRMS techniques (see Fig. S3, ESI), showing identical major species and fragmentation patterns.

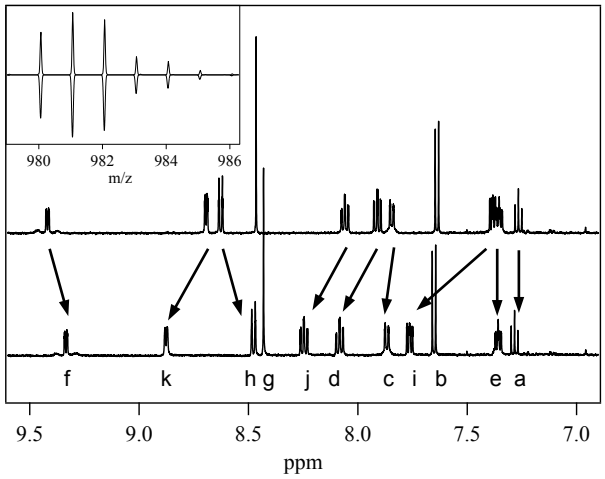

Figure 2: ^{1}H NMR spectrum of Pt(II) metalloligand [Pt(N^C^N)(a-tpy)] (top) and corresponding Lu(III) complex (bottom), with individual resonances assigned according to the labels in Scheme 1. Inset: HRMS (ESI+) showing observed isotopic distribution (top) and calculated spectrum (bottom) for $[Pt(N^C^N)(a\text{-}tpy)Lu(NO_3)_2]^+$.

Steady-state photophysics

Initial photophysical characterisation of our a-tpy substituted Pt(II) metalloligand was undertaken in CH_2Cl_2 solution by a comparison to the parent [Pt(N^C^N)Cl] complex. The UV-Vis spectrum of the [(N^C^N)Pt(a-tpy)] complex (Fig. S4, ESI) shows an increase in high-energy, ligand-centred transitions

centred at *ca*. 290 nm, attributed to the presence of the additional a-tpy ligand, whereas the lower energy transitions between *ca.* 350-450 nm show comparatively slight differences compared to the parent [Pt(N^C^N)Cl] complex. This region of the absorption spectrum has been assigned to $d_{Pt}|\pi_{NCN} \rightarrow \pi^*_{NCN}$ transitions for the parent complex.[19b] Accordingly, both complexes display almost identical phosphorescence emission spectra upon excitation at 385 nm, as shown in Fig. S4, ESI. Vibrationally resolved spectra with similar 0,0 components at 491 and 495 nm for the parent and terpyridyl appended complexes respectively are observed for both complexes. The solution PLQY (Φ) values in aerated CH_2Cl_2 are 3.9 and 3.8±0.8 % respectively. Interestingly, despite their similar PLQYs, the a-tpy substituted Pt(II) metalloligand has a much shorter lifetime (τ = 252 ns) compared to the reported value (τ = 500 ns) of the parent [Pt(N^C^N)Cl] complex under the same conditions. Using this data, the radiative (k_r) and non-radiative (k_{nr}) decay rates were evaluated (see Table S1, ESI) and indicate an increase in both these values for the a-tpy substituted complex. While the latter is likely due the presence of additional vibrational modes (e.g. –C≡C–) and/or differing rates of quenching by molecular oxygen, the increase in k_r can instead be attributed to the difference in the metal's coordination sphere. Interestingly, a comparison of calculated decay rates using data previously reported[23] for the [Pt(N^C^N)Cl] and [Pt(N^C^N)L] complexes in degassed CH_2Cl_2 solution (where L is a coordinated alkyne-phenyl ligand) reveals similar increases in k_r and k_{nr}.

Since the $^6P_{7/2}$ excited state of Gd(III) is considerably higher in energy than the lowest excited states of the Pt(II) metalloligand, energy transfer to the 4*f** excited states for this metal as an acceptor is essentially impossible at ambient temperature, and the Pt(II)-Gd(III) complex serves as a good model for the influence of coordinated Ln(III) cations on the photophysical properties of the metalloligand. Upon complexation of Ln(III) cations to the free a-tpy group of the Pt(II) metalloligand, some notable changes were evident in the steady state photophysics. As shown in Fig. 3, a comparison of the UV-Vis spectra for the Pt(II) metalloligand and [Pt(N^C^N)(a-tpy)Gd$(NO_3)_3$] complex in CH_3CN solution reveal a slight sharpening of the ligand centred transition in the UV at *ca.* 290 nm, as well as an increase in absorption intensity at wavelengths greater than *ca*. 300 nm. We attribute the latter to a shifted a-tpy centered π-π* absorption band upon Ln(III) complexation, which comparatively appears between 300-350 nm for free tpy,[24] while the smaller increase at *ca*. 420 nm is in the expected region for the charge transfer (^{1}CT) bands of the Pt(II) complex. Identical changes in the absorption spectra were also observed upon complexation with the other Ln(III) cations (see Fig. S5, ESI). Interestingly, while coordination of the Gd(III) cation has no influence on the spectral profile of the Pt(II)-metalloligand phosphorescence, there is a significant reduction in the emission intensity, with a PLQY for the free metalloligand of Φ = 1.0 ± 0.1 % in CH_3CN solution, which is reduced to Φ = 0.1 ± 0.01 % for the Gd(III) *d-f* complex.

Sensitised Ln(III) luminescence

Coordination of the Ln(III) cations Nd, Yb and Er, which possess low energy 4*f** excited states, allowed for sensitised NIR emission to be observed, as shown in Fig. 3. These metal ions are able to act as energy transfer acceptors, with the excited triplet state of the [Pt(N^C^N)(a-tpy)] metalloligand acting as energy donor. Hence, using excitation at λ_{ex} = 420 nm, which corresponds to the low energy maximum of the ^{1}CT absorption band, several characteristic NIR emission bands were observed. Specifically, for Yb(III), emission at 980 nm corresponds to the $^2F_{5/2} \rightarrow {}^2F_{7/2}$ transition, while for Er(III), the observed $^4I_{13/2} \rightarrow {}^4I_{15/2}$ emission band appears at 1530 nm. For the Nd(III) complex, three bands are observed at *ca*. 890, 1060 and 1335 nm respectively, which can be attributed to the $^4F_{3/2} \rightarrow {}^4I_J$ (J = 9/2, 11/2, 13/2) transitions respectively. To quantify the NIR emission intensity, the PLQY for the Yb(III) centered emission from [Pt(N^C^N)(a-tpy)Yb$(NO_3)_3$] was determined, using [Yb$(tta)_3$(phen)] as a suitable NIR PLQY standard[25] (Φ = 1.6 % in aerated toluene), yielding a value of Φ = 0.46 ± 0.04 %, which is comparable to other substituted 2,2':6',2''-terpyridine Yb(III) tris-nitrato complexes.[26]

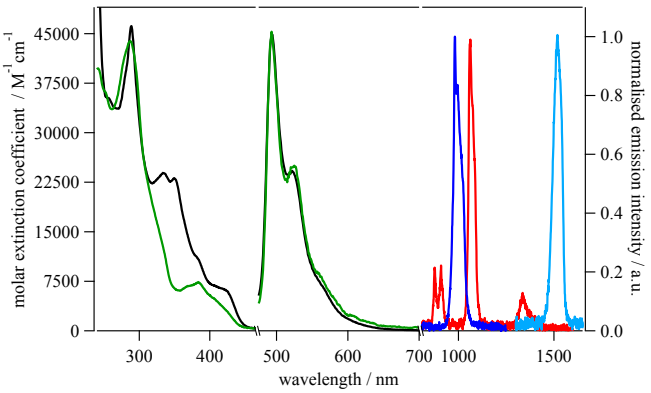

Figure 3: UV-Vis (left axis) of Pt(II) metalloligand (green) and corresponding Gd(III) complex (black). Normalised emission (right axis) of Pt(II) metalloligand (green) and [Pt(N^C^N)(a-tpy)Ln$(NO_3)_3$] complexes with Ln = Gd (black), Nd (red), Yb (blue) and Er (cyan).

Density Functional Theory

In order to gain a more detailed understanding of the nature of the excited states for both the [Pt(N^C^N)(a-tpy)] metalloligand and the bimetallic 4*f* complexes, we have undertaken both static and Time Dependent Density Functional Theory (TD-DFT) calculations using mixed B3LYP 6-31g* and LANL2DZ basis sets. However, to avoid computationally expensive calculations involving the 4*f* metal ions, we utilised a diamagnetic Y(III) cation to give a simpler model complex, since this metal has an identical charge and similar ionic radius to the Ln(III) cations. We have previously found this to be a very useful approach for understanding ligand-centered electronic structures.[22]

The resulting optimised geometries and frontier molecular orbitals for the [Pt(N^C^N)(a-tpy)] metalloligand and corresponding Y(III) complex are shown in Fig. 4. For the former, the resulting geometry obtained is very similar to the structure obtained by X-ray crystallography. In particular, the N^C^N and a-tpy ligands are coplanar, and the pattern of Pt-N and Pt-C bond lengths around the metal ion is reproduced. Also, the N donor atoms of the a-tpy ligand adopt a *trans-trans* configuration, as observed crystallographically. For the corresponding Y(III) complex, the coordination geometry about the Pt(II) centre is square planar, and the pattern of Pt-N and Pt-C bond lengths again matches our expectations based on the strong *trans* influence of the organometallic N^C^N ligand. The calculated geometry around the Y(III) cation is as expected, showing tridentate coordination of the a-tpy ligand, and three coordinated nitrate anions, all of which are bidentate, with one lying

approximately opposite the metal ion, and the remaining two occupying sites above and below the plane of the a-tpy ligand. Perhaps most interestingly, the high degree of planarity observed in the [Pt(N^C^N)(a-tpy)] metalloligand is disrupted in the calculated structure of the Y(III) complex, with the organic N^C^N and a-tpy ligands instead adopting an essentially orthogonal disposition (showing a bond torsion of 90.1° between the a-tpy and Pt(N^C^N) planes) which may have important implications for the resulting electronic structure.

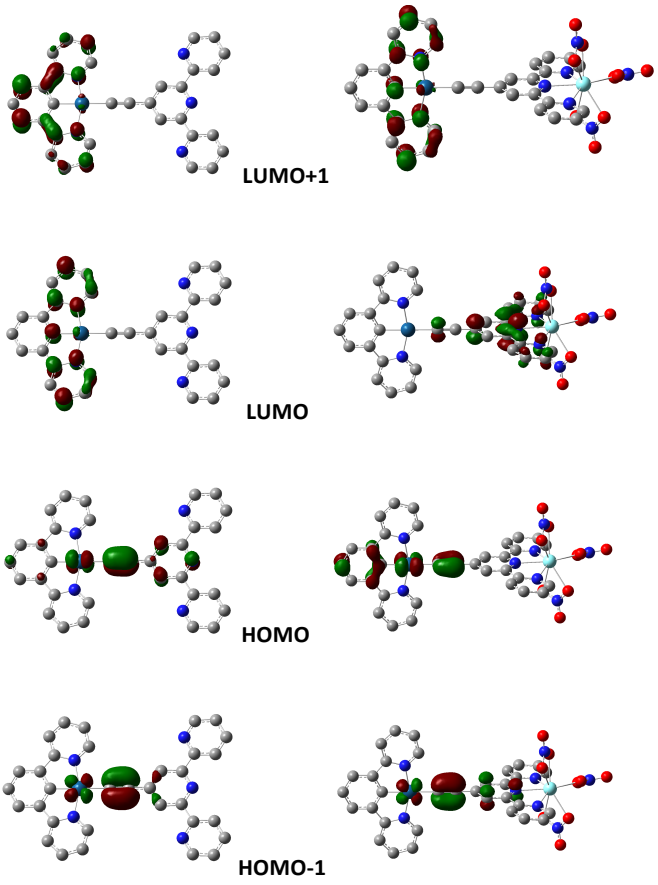

Figure 4: Optimised DFT geometries of [Pt(N^C^N)(a-tpy)] (left) and [Pt(N^C^N)(a-tpy)Y(NO_3)$_3$] (right) and selected molecular orbitals.

For both the metalloligand and the bimetallic complex, it is clear that the excited state transitions have mixed parentage, and can best be described as metal-perturbed interligand (ILCT) charge transfer states, since π orbitals of both the N^C^N and a-tpy ligands are involved. For the [Pt(N^C^N)(a-tpy)] complex, the lowest energy singlet (S_1) and triplet (T_1) excited state transitions predominantly involve the HOMO and LUMO orbitals, which are co-localised on the alkyne (σ)/Pt(II) (d) center of the a-tpy ligand and the N^C^N ligand (π*) respectively (see Table S2, ESI). For the corresponding bimetallic Pt(II)/Y(III) complex, the lowest energy S_1 and T_1 excited state transitions predominantly involve the HOMO and LUMO+1 molecular orbitals, although the latter also has a significant (25.8%) HOMO-1 → LUMO contribution. This is interesting, since although the HOMO and LUMO+1 are again alkyne (σ)/Pt(II) (d) and N^C^N (π*) ligand based respectively, the calculated LUMO is clearly localised on the a-tpy ligand, with π* character. The same HOMO-1 → LUMO transition is also significant for the T_2 excited state, which is very similar in energy, and suggests the presence of a metal perturbed π-π* excited state localised over the terpyridine end of the a-tpy ligand, which is not present in the free metalloligand. Localisation of the excited state closer to the 4*f* metal ion would enhance the rate of EET from metalloligand to coordinated Ln(III) cation, due to the much shorter distances involved. Nonetheless, the similarity observed between the visible emission spectra of the [Pt(N^C^N)(a-tpy)] metalloligand and the corresponding Gd(III) complex (Fig. 3) is consistent with the HOMO → LUMO+1 being the main contributor to the lowest energy T_1 state in the *d-f* complexes.

Excited state dynamics

The excited-state lifetimes for several of the Pt(II)-Ln(III) complexes were determined using a combination of ns- and fs-TA spectroscopy. The resulting fs-TA spectra for the Er(III) complex are shown in Fig. 5a, with data for the remaining complexes given in the supporting information (see Figs. S6, ESI). Upon excitation (λ_{ex} = 420 nm), rapid formation of a positive excited state absorption (ESA) band centered at *ca*. 500 nm is apparent in all complexes, which we attribute to $T_1 \rightarrow T_n$ transitions of the lowest energy triplet excited state. The multiplicity of this state as a triplet was also confirmed by corresponding measurements in degassed solution, which yielded considerably longer excited state lifetimes (Fig S6, ESI). Similarly, negative Ground State Bleach (GSB) signals were observed at *ca*. 360, 385 and 420 nm. We do not observe any evidence for $S_1 \rightarrow S_n$ transitions of the initially populated singlet excited state, which presumably undergoes very rapid ISC within the IRF of our experimental setup (*ca.* 200 fs). This is to be expected, given the likelihood of enhanced spin orbit coupling due to the Pt(II) metal ion, which favours very fast $S_1 \rightarrow T_1$ intersystem crossing.

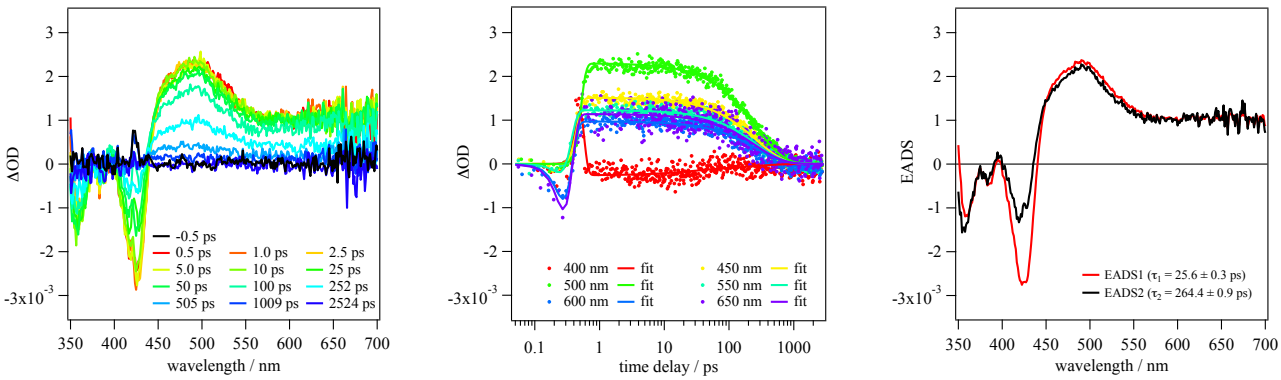

Figure 5: (a) Observed femtosecond Transient Absorption (fs-TA) spectra at selected time delays as shown for [Pt(N^C^N)(a-tpy)Er(NO_3)$_3$] in CH_3CN (λ_{ex} = 420 nm), (b) corresponding decay kinetics and global fits at selected wavelengths as indicated and (c) resulting Evolution Associated Difference Spectra (EADS) and lifetime summary from global fitting analysis (see text for details).

Table 1. Summary of the excited-state lifetimes for the [Pt(N^C^N)(a-tpy)Ln(NO_3)$_3$] complexes (Ln = Gd, Nd, Er and Yb) in CH_3CN solution (λ_{ex} = 420 nm) obtained by a combination of fs-TA and ns-TA experiments

Complex	τ_1 (ps)	k_{obs} (s^{-1})	τ_2 (ns)	k_{obs} (s^{-1})	k_{EET} (s^{-1})	Φ_{EET} (%)
[Pt(N^C^N)(a-tpy)Gd(NO_3)$_3$]	37.7 ± 0.6	2.65×10^{10}	9590 ± 18.5	1.04×10^{8}	N/A	N/A
[Pt(N^C^N)(a-tpy)Nd(NO_3)$_3$]	39.9 ± 0.6	2.51×10^{10}	237.3 ± 1.2	4.21×10^{9}	4.11×10^{9}	97.5
[Pt(N^C^N)(a-tpy)Er(NO_3)$_3$]	25.6 ± 0.4	3.91×10^{10}	264.3 ± 0.9	3.78×10^{9}	3.68×10^{9}	97.2
[Pt(N^C^N)(a-tpy)Yb(NO_3)$_3$]	34.3 ± 0.4	2.92×10^{10}	1991.4 ± 7.0	5.02×10^{8}	3.98×10^{8}	79.2

The kinetic decays of the observed GSB and ESA signals were fitted globally using the GloTarAn software package and the R package TIMP.[27] It was found that a sequential biexponential decay model summarised by the equation;

$$I_{(t)} = A_1 \exp^{-\tau 1(t)} + A_2 \exp^{-\tau 2(t)} \quad (1)$$

gave an excellent fit to the experimental data, where $\tau_{1\text{-}2}$ represent exponential decay times, and $A_{1\text{-}2}$ are pre-exponential scaling factors. A summary of the determined lifetimes is given in Table 1, and the agreement between the global fit results and the experimental data is demonstrated in Fig. 5b for the [Pt(N^C^N)(a-tpy)Er(NO_3)$_3$] complex, with corresponding data for the other Ln(III) complexes given in the Supporting Information (see Figs S6, ESI). In all cases, a short lived component ($\tau_1 \approx 30$ ps) was observed, followed by a much longer lived species, with τ_2 ranging from *ca*. 200 ps to 9.6 ns, depending on the identity of the chelated 4*f* metal ion. Analysis of the corresponding Evolution Associated Difference Spectra (EADS) shown in Fig. 5c reveals the very close similarity obtained for EADS1 and EADS2, apart from a subtle blue shift for the latter. Hence, we assign the initially observed species to a vibrationally excited state, which rapidly thermalises to the lowest energy excited triplet state. In accordance with the TD-DFT calculations, it likely has a mixture of metal perturbed ILCT and ππ* character.

Antenna pathway and efficiency

Using transient absorption spectroscopy, the excited state dynamics of the bimetallic complexes have been elucidated. Upon excitation via the singlet intraligand charge transfer (^{1}ILCT) transition at *ca* 420 nm, the corresponding lowest energy triplet excited state, which has mixed ^{3}ILCT / ^{3}ππ* parentage, is rapidly formed by a highly efficient intersystem crossing (ISC) process, on a timescale faster than the available resolution of our experimental setup at ca. 200 fs. After thermalisation of this triplet state, subsequent ^{3}ILCT / ^{3}ππ* lifetimes range from 9.59 ns for the Pt(II)-Gd(III) complex to as low as *ca*. 240 ps for the Pt(II)-Nd(III) complex.

The significant decrease in the ^{3}ILCT / ^{3}ππ* lifetime for the NIR emissive Ln(III) complexes compared to Gd(III) can be attributed to quenching by EET from the metalloligand to the bound Ln(III) metal ions. Notably, since Gd(III) cannot act as an energy acceptor, the excited state lifetime for the [Pt(N^C^N)(a-tpy)Gd(NO_3)$_3$] complex serves as a suitable model to calculate the rate (k_{EET}) and efficiency (Φ_{EET}) of the energy transfer process using the equations:[28, 29]

$$k_{EET} = 1/\tau_q - 1/\tau_u \quad (2)$$

$$\Phi_{EET} = 1 - \tau_q/\tau_u \quad (3)$$

where τ_q and τ_u are the evaluated triplet lifetimes in the presence and absence of quencher, which in this case are the Nd(III), Er(III) and Yb(III) cations that are capable of accepting energy.

As summarised in Table 1, the calculated rates we obtain for k_{EET} are on the order of 10^8-10^9 s^{-1}, with corresponding efficiencies from *ca*. 80 to almost 100%, suggesting the antenna effect pathway in these heterobimetallic *d-f* complexes is very efficient. Notably, much higher values were obtained for k_{EET} in the Nd(III) and Er(III) complexes (and hence higher Φ_{EET}) which can be rationalised by an improved spectral overlap between the emission spectrum of the metalloligand donor and the absorption bands of the accepting 4*f* cations. Specifically, both the Nd(III) and Er(III) cations have multiple excited state levels which overlap with the donating ^{3}ILCT / ^{3}ππ* state of the metalloligand, and may act as acceptors, allowing for rapid and efficient energy transfer. Conversely, for the Yb(III) cation, there is only a single excited state which is considerably lower in energy, resulting in a much poorer overlap and hence less efficient EET.

Conclusions

A novel cyclometallated Pt(II) metalloligand bearing a free alkyne-tpy binding unit for Ln(III) cations has been synthesised and fully characterised. Moreover, the photophysical properties of both the parent complex and a series of corresponding heterobimetallic *d-f* complexes have been investigated. The [Pt(N^C^N)(a-tpy)] complex was found to have very similar properties to the parent [Pt(N^C^N)Cl] complex, including bright phosphorescence and a long lived triplet excited state.

Corresponding photoluminescence properties of the bimetallic [Pt(N^C^N)(a-tpy)Ln(NO_3)$_3$] complexes with Ln(III) = Nd, Er and Yb were also explored, and demonstrate relatively intense NIR emission from the 4*f* cation in each case. Interestingly, TD-DFT studies suggest a change in the excited state localisation upon coordination of the 4*f* cation, with the lowest energy triplet showing a small amount of $^3\pi\pi^*$ character on the ethynyl-terpyridine end of the complex. The resulting NIR emission was shown to be sensitised with exceptionally high efficiencies, which have been characterised using ultrafast spectroscopic techniques.

Experimental

General

All starting reagents and solvents were used as supplied from commercial suppliers (Sigma Aldrich, Alpha Aesar, Strem Chemicals, Scharlau). The [Pt(N^C^N)Cl] complex was prepared as previously reported.[30] ^{1}H NMR spectra were acquired using a Bruker AV500 spectrometer operating at 500 MHz. Observed signals were referenced to the residual solvent peak (CD_3CN, δ = 1.93 ppm) and spectra were processed using the Topspin Plot Editor and MestRe Nova software packages. Elemental analyses (CHN) were performed using a Thermo Scientific Flash 2000 Organic Elemental Analyser at the Micro-Analytical unit at the School of Chemistry and Molecular Biosciences (UQ). High Resolution Mass Spectrometry (HRMS) data were collected using a Thermo-Fisher Orbitrap Elite mass spectrometer operating in electrospray positive ion (ESI+) mode.

Synthesis

[(N^C^N)Pt(a-tpy[1])]

[Pt(N^C^N)Cl (0.05 g, 0.108 mmol) was dissolved in a mixture of methanol-dichloromethane (4:1 v/v, 50 mL) and then added to a Schlenk tube containing 4'-ethynyl-terpyridine (0.0279 g, 0.108 mmol) and sodium methoxide (0.006 g, 0.110 mmol) dissolved in methanol (15 mL). The solution was left to stir for 4 hours under an N_2 atmosphere at room temperature, then the resulting precipitate was washed and centrifuged with H_2O and methanol to give the desired complex as a yellow powder (0.070 g, 0.1 mmol, 94% yield). Found: C, 57.41; H, 3.01; N, 9.96. Calc. for $C_{33}H_{21}N_5Pt{\cdot}0.5(H_2O)$: C, 57.31; H, 3.21; N, 10.13). ^{1}H NMR (500 MHz, CD_2Cl_2) δ 9.48 (ddd, *J* = 5.7, 1.7, 0.8 Hz, 2H), 8.71 (ddd, *J* = 4.8, 1.8, 0.9 Hz, 3H), 8.64 (dt, *J* = 8.0, 1.1 Hz, 3H), 8.52 (s, 2H), 8.00 (ddd, *J* = 8.0, 7.6, 1.7 Hz, 3H), 7.88 (ddd, *J* = 8.0, 7.5, 1.8 Hz, 3H), 7.76 (s, 1H), 7.76 (ddd, *J* = 8.0, 1.5, 0.7 Hz, 2H), 7.60 (d, *J* = 7.6 Hz, 3H), 7.41 – 7.23 (m, 7H). HRMS (ESI+): *m/z* 683.15 M-H$^+$ (683.15, 100%) (684.15, 85%) (682.15, 71%) (685.16, 26%) (686.16, 19%)

[(N^C^N)Pt(a-tpy)Ln(NO_3)$_3$]

Solutions of [Pt(N^C^N)(a-tpy)Ln(NO_3)$_3$] complexes were prepared by suspending the isolated [(N^C^N)Pt(a-tpy)] complex in CH_3CN at 298 K, followed by addition of a slight excess (1.1 mol %) of the requisite Ln(NO_3)$_3$.*x*H_2O salt (Ln = Nd, Gd, Er, Yb, *x* = 6). Resulting solutions of the heterobimetallic complexes were characterised by ^{1}H NMR (for diamagnetic Ln^{3+}) and HRMS (ESI+) analysis to confirm their formulation.

[(N^C^N)Pt(a-tpy)Lu(NO_3)$_3$]

^{1}H NMR (500 MHz, CD_3CN) δ 9.42-9.37 (m, 1H), 8.95-8.90 (m, 2H), 8.59 (d, *J* = 8.1 Hz, 2H), 8.52 (s, 2H), 8.35 – 8.28 (m, 2H), 8.16 (td, *J* = 7.8, 1.6 Hz, 2H), 7.95 (d, *J* = 8.0 Hz, 2H), 7.83 (ddd, *J* = 7.6, 5.4, 1.1 Hz, 2H), 7.73 (d, *J* = 7.7 Hz, 2H), 7.44 (ddd, *J* = 7.3, 5.7, 1.5 Hz, 2H), 7.34 (t, *J* = 7.7 Hz, 1H). HRMS (ESI+): *m/z* [N^C^N)Pt(a-tpy)Lu(NO_3)$_2$]$^{1+}$ (981.07, 100%) (982.07, 89%) (980.06, 69%) (983.07, 30%) (984.07, 22%)

Crystallography

Data for **[(N^C^N)Pt(a-tpy)]** were collected on an Oxford Gemini Ultra diffractometer with graphite monochromated MoK_α radiation (λ = 0.71073), and operating in the ω-2Θ scan mode at 190 K. Data reduction, integration and empirical absorption correction (ψ-scans) were performed with CrysAlisPro.[31] and subsequent computations were carried out using *OLEX-2*.[32] The structure solution was obtained using *SHELXT*[33] and a full matrix least-squares refinement was carried out with *SHELXL*[34] through the *OLEX-2* interface. Reflections at angles greater than 50° 2ϑ were omitted, and non-H atoms were refined using anisotropic displacement parameters. The CIF file has been deposited with the CSD (CCDC reference number 1880816).

Crystal Data for $C_{33}H_{21}N_5Pt$ (M =682.64 g/mol): monoclinic, space group $P2_1/c$ (no. 14), a = 15.1953(8) Å, b = 11.9962(6) Å, c = 14.2787(8) Å, β = 103.940(5)°, V = 2526.1(2) Å^3, Z = 4, crystal dimensions 0.1 x 0.085 x 0.05 mm, colour yellow, habit block, T = 190(2) K, μ(Mo$K\alpha$) = 5.588 mm^{-1}, D_{calc} = 1.795 g/cm^3, 12635 reflections measured (6.776° ≤ 2ϑ ≤ 52.738°), 5146 unique (R_{int} = 0.0649, R_{sigma} = 0.0833) which were used in all calculations. The final R_1 was 0.0420 ($I > 2\sigma(I)$), wR_2 was 0.0814 (all data) and GoF on F^2 was 1.015(all data).

Photophysics

Steady state and time-resolved photophysical experiments were performed using quartz cuvettes of 1 cm and 0.2 cm path lengths respectively. UV-Visible absorption spectra were recorded using an Agilent Cary 60 UV-Vis spectrometer with the Cary WinUV Scan application (Version 5.0.0.999). Emission spectra were measured using a HORIBA Jobin Yvon IBH FluoroLog-311 spectrofluorimeter and the FluorEssence (Version 3.1.5.11) software package. All emission spectra were reference corrected for the light source variation (lamp and grating) and the emission spectral response (detector and grating). Spectrophotometric data were processed using Igor (Wavemetrics, Inc, Version 6.1.1.2). Femtosecond and nanosecond transient absorption (TA) measurements were collected using an amplified fs laser system as previously reported[35]

with subsequent data analysis performed using GloTarAn and the R package TIMP.[27] For steady state emission and TA measurements, the absorbance of samples was in the range 0.2–0.5 at the excitation wavelength.

Conflicts of interest

There are no conflicts to declare.

Acknowledgements

Financial support by the Australian Research Council (ARC) is gratefully acknowledged (DP170101895). I.M.E. gratefully acknowledges the award of an M.G. and R. A. Plowman scholarship from SCMB (UQ), which funded parts of this research project undertaken at the University of Durham.

Notes and references

1. S. I. Klink, H. Keizer and F. C. J. M. van Veggel, *Angew. Chem. Int. Ed.*, 2000, **39**, 4319-4321.
2. M. D. Ward, *Coord. Chem. Rev.*, 2007, **251**, 1663-1677.
3. T. K. Aldridge, E. M. Stacy and D. R. McMillin, *Inorg. Chem.*, 1994, **33**, 722-727.
4. D. K. Crites, C. T. Cunningham and D. R. McMillin, *Inorg. Chim. Acta*, 1998, **273**, 346-353.
5. H.-K. Yip, L.-K. Cheng, K.-K. Cheung and C.-M. Che, *J. Chem. Soc., Dalton Trans.*, 1993, 2933-2938.
6. P. Kadjane, C. Platas-Iglesias, R. Ziessel and L. J. Charbonnière, *J. Chem. Soc., Dalton Trans.*, 2009, 5688-5700.
7. F. Kennedy, N. M. Shavaleev, T. Koullourou, Z. R. Bell, J. C. Jeffery, S. Faulkner and M. D. Ward, *J. Chem. Soc., Dalton Trans.*, 2007, 1492-1499.
8. R. Ziessel, S. Diring, P. Kadjane, L. Charbonnière, P. Retailleau and C. Philouze, *Chem. Asian J.*, 2007, **2**, 975-982.
9. T. K. Ronson, T. Lazarides, H. Adams, S. J. A. Pope, D. Sykes, S. Faulkner, S. J. Coles, M. B. Hursthouse, W. Clegg, R. W. Harrington and M. D. Ward, *Chem. Eur. J.*, 2006, **12**, 9299-9313.
10. P. B. Glover, P. R. Ashton, L. J. Childs, A. Rodger, M. Kercher, R. M. Williams, L. De Cola and Z. Pikramenou, *J. Am. Chem. Soc.*, 2003, **125**, 9918-9919.
11. X.-L. Li, L.-X. Shi, L.-Y. Zhang, H.-M. Wen and Z.-N. Chen, *Inorg. Chem.*, 2007, **46**, 10892-10900.
12. H.-B. Xu, L.-X. Shi, E. Ma, L.-Y. Zhang, Q.-H. Wei and Z.-N. Chen, *Chem. Commun.*, 2006, 1601-1603.
13. K.-J. Chen, H.-B. Xu, L.-Y. Zhang and Z.-N. Chen, *Inorg. Chem. Commun.*, 2009, **12**, 744-746.
14. O. J. Stacey, A. J. Amoroso, J. A. Platts, P. N. Horton, S. J. Coles, D. Lloyd, C. F. Williams, A. J. Hayes, J. J. Dunsford and S. J. A. Pope, *Chem. Commun.*, 2015, **51**, 12305-12308.
15. Y. Chen, K. Li, W. Lu, S. S.-Y. Chui, C.-W. Ma and C.-M. Che, *Angew. Chem. Int. Ed.*, 2009, **48**, 9909-9913.
16. S. Develay and J. A. G. Williams, *J. Chem. Soc., Dalton Trans.*, 2008, 4562-4564.
17. Z. Wang, E. Turner, V. Mahoney, S. Madakuni, T. Groy and J. Li, *Inorg. Chem.*, 2010, **49**, 11276-11286.
18. S. J. Farley, D. L. Rochester, A. L. Thompson, J. A. K. Howard and J. A. G. Williams, *Inorg. Chem.*, 2005, **44**, 9690-9703.
19. (a) J. A. G. Williams, A. Beeby, E. S. Davies, J. A. Weinstein and C. Wilson, *Inorg. Chem.*, 2003, **42**, 8609-8611. (b) D. L. Rochester, S. Develay, S. Zalis and J. A. G. Williams, *Dalton Trans.* 2009, 1728-1741.
20. V. Grosshenny, F. M. Romero and R. Ziessel, *J. Org. Chem.*, 1997, **62**, 1491-1500.
21. E. Rossi, A. Colombo, C. Dragonetti, D. Roberto, R. Ugo, A. Valore, L. Falciola, P. Brulatti, M. Cocchi and J. A. G. Williams, *J. Mater. Chem.*, 2012, **22**, 10650-10655.
22. E. G. Moore, M. Benaglia, G. Bergamini and P. Ceroni, *Eur. J. Inorg. Chem.*, 2015, 414-420.
23. C. Yong, L. Kai, L. Wei, C. S. Sin-Yin, M. Chun-Wah and C. Chi-Ming, *Angew. Chem. Int. Ed.*, 2009, **48**, 9909-9913.
24. J. M. Hamilton, M. J. Anhorn, K. A. Oscarson, J. H. Reibenspies and R. D. Hancock, *Inorg. Chem.*, 2011, **50**, 2764-2770.
25. M. P. Tsvirko, S. B. Meshkova, V. Y. Venchikov, Z. M. Topilova and D. V. Bol'shoi, *Opt. Spectrosc.*, 2001, **90**, 669-673.
26. R. F. Ziessel, G. Ulrich, L. Charbonnière, D. Imbert, R. Scopelliti and J.-C. G. Bünzli, *Chem. Eur. J.*, 2006, **12**, 5060-5067.
27. J. J. Snellenburg, S. P. Laptenok, R. Seger, K. M. Mullen and I. H. M. van Stokkum, *J. Stat. Softw.*, 2012, **49**, 1-22.
28. S. Faulkner, L. S. Natrajan, W. S. Perry and D. Sykes, *J. Chem. Soc., Dalton Trans.*, 2009, 3890-3899.
29. T. Lazarides, D. Sykes, S. Faulkner, A. Barbieri and M. D. Ward, *Chem. Eur. J.*, 2008, **14**, 9389-9399.
30. D. J. Cárdenas, A. M. Echavarren and M. C. Ramírez de Arellano, *Organometallics*, 1999, **18**, 3337-3341.
31. *CrysAlisPro*, Oxford Diffraction Ltd: Abingdon, Oxfordshire, England, 2007.
32. O. V. Dolomanov, L. J. Bourhis, R. J. Gildea, J. A. K. Howard and H. Puschmann, *J. Appl. Cryst.*, 2009, **42**, 339-341.
33. G. Sheldrick, M., *Acta Cryst.*, 2015, **A71**, 3-8.
34. G. M. Sheldrick, *SHELX-2014: Programs for Crystal Structure Analaysis*, University of Göttingen, Göttingen, 2014.
35. B. S. K. Chong and E. G. Moore, *Inorg. Chem.*, 2018, DOI: 10.1021/acs.inorgchem.8b01438.